Available online at www.sciencedirect.com
SCIENCE DIRECT®
International Journal of Heat and Fluid Flow 24 (2003) 669–679
International Journal of HEAT AND FLUID FLOW
www.elsevier.com/locate/ijhff

The effect of freestream turbulence on film cooling adiabatic effectiveness

James E. Mayhew [a,*], James W. Baughn [b], Aaron R. Byerley [c]

[a] Department of Mechanical Engineering, Rose-Hulman Institute of Technology, 5500 Wabash Avenue, Terre Haute, IN 47803, USA
[b] Mechanical and Aeronautical Engineering, University of California, Davis, CA, USA
[c] Department of Aeronautics, US Air Force Academy, Colorado Springs, CO, USA

Received 19 September 2002; accepted 29 April 2003

Abstract

The film-cooling performance of a flat plate in the presence of low and high freestream turbulence is investigated using liquid crystal thermography. This paper contributes high-resolution color images that clearly show how the freestream turbulence spreads the cooling air around a larger area of the film-cooled surface. Distributions of the adiabatic effectiveness are determined over the film-cooled surface of the flat plate using the hue method and image processing. Three blowing rates are investigated for a model with three straight holes spaced three diameters apart, with density ratio near unity. High freestream turbulence is shown to increase the area-averaged effectiveness at high blowing rates, but decrease it at low blowing rates. At low blowing ratio, freestream turbulence clearly reduces the coverage area of the cooling air due to increased mixing with the main flow. However, at high blowing ratio, when much of the jet has lifted off in the low turbulence case, high freestream turbulence turns its increased mixing into an asset, entraining some of the coolant that penetrates into the main flow and mixing it with the air near the surface.

Keywords: Adiabatic effectiveness; Film cooling; Freestream turbulence; Liquid crystal

1. Introduction

Film cooling is a process used to cool turbine blades in gas turbine engines. The temperature of the hot gas stream in the turbine is high enough to damage the metal blades without film cooling. Film-cooling air first flows through passageways inside the blade, then flows out through the film cooling holes. Ideally the cooling air remains close to the blade surface and in effect forms a protective blanket to shield the blade from the hot gas stream. However, under some circumstances, the cooling air shoots out into the hot gas stream and provides little to no protection to the blade surface. Clearly, it is important for turbine designers to know the circumstances under which the cooling air will provide good protection to the blade.

Since the flow in a gas turbine engine typically has freestream turbulence on the order of 10–20% in the regions where film cooling is employed, it is important to study how this freestream turbulence affects film cooling performance. The extent to which the film-cooling mechanisms observed in experiments with low freestream turbulence are relevant to high freestream turbulence flows is unclear. Following is a brief review of other researchers' efforts to understand these effects, as well as the objectives of the current research.

1.1. Film cooling adiabatic effectiveness

Several research teams have found the adiabatic effectiveness on a film-cooled flat plate in a low turbulence environment. Schmidt et al. (1996) and Sen et al. (1996) are companion papers reporting the adiabatic effectiveness and heat transfer coefficient, respectively, of a flat plate with a straight hole and a compound angle hole. Their experiments were conducted in a low Tu (~0.2%) wind tunnel. One contribution of theirs was to note that film-cooling performance can be characterized by the net heat flux reduction (NHFR), rather than the adiabatic effectiveness alone. The NHFR includes the effects of adiabatic effectiveness and accounts for changes in

* Corresponding author. Tel.: +812-877-8917; fax: +812-877-8025.
E-mail address: mayhew@rose-hulman.edu (J.E. Mayhew).

0142-727X/$ - see front matter © 2003 Elsevier Inc. All rights reserved.
doi:10.1016/S0142-727X(03)00081-X

Nomenclature

A	area (m^2)
B	bias (systematic) uncertainty, 95% confidence, or blue
D	diameter of film-cooling hole
DR	density ratio, ρ_{jet}/ρ_∞
G	green
I	momentum flux ratio, $\rho_{jet}V_{jet}^2/\rho_\infty V_\infty^2$
M	blowing ratio, $\rho_{jet}V_{jet}/\rho_\infty V_\infty$
P	random uncertainty, 95% confidence
T	temperature (°C or K)
Tu	turbulence intensity
U	uncertainty
V	velocity (m/s)
h	convective heat transfer coefficient (W/m^2 K)
k	thermal conductivity (W/m K)
x	streamwise dimension
z	spanwise dimension

Greeks

δ_1	boundary layer displacement thickness
η	adiabatic effectiveness
ρ	density (kg/m^3)
θ	boundary layer momentum thickness

Subscripts

aw	adiabatic wall
jet	film-cooling air jet
p	plenum
r	radiation heat transfer
∞	freestream

heat transfer coefficient as a result of the film cooling. They found that the compound angle improved the effectiveness. Their results are used later for comparison to the present results.

Kohli and Bogard (1997) report on the film cooling effectiveness on a flat plate using 35° and 55° injection angles. They also report on the thermal and velocity fields in the region around the injection holes.

Walters and Leylek (1997) performed numerical analyses on a film-cooled flat plate geometry in a low freestream turbulence environment. They use their computations in conjunction with experimental data in order to help explain the key underlying physics associated with film-cooling flow fields, emphasizing that their turbulence models do not need to be "perfect" in order to do this. They report that the most significant mechanism affecting film-cooling performance is the counter-rotating secondary flow structure downstream of the jet exit. The companion papers (McGovern and Leylek, 1997; Hyams and Leylek, 1997; Brittingham and Leylek, 1997) continue this investigation for different injection angles and hole shapes.

1.2. Effectiveness at high freestream turbulence

Relatively few researchers have examined the effect of freestream turbulence on film cooling effectiveness. Bons et al. (1994) found the adiabatic effectiveness along the centerline of three film cooling holes by measuring adiabatic wall temperatures with thermocouples embedded beneath the surface of their flat plate model. Their results show that high freestream turbulence (Tu) decreases effectiveness when the film cooling air is at a low blowing ratio (M), but increases effectiveness at high M. They postulate that, for the low Tu – low M case, the cooling air remains near the surface and cools it well. When high freestream turbulence is introduced, it removes much of this cooling air from near the surface and mixes it with the freestream, resulting in less cooling air near the surface and therefore lower effectiveness. For the low Tu – high M case, they argue that the cooling air lifts off from the surface as it leaves the hole, and therefore does little good. High Tu mixes this lifted-off air and brings some of it back near the surface, improving the effectiveness. They found this effect to be strongly dependent on the blowing ratio. They also found the effectiveness along a line midway between the cooling holes. Along this midway line, the effectiveness is very low until the cooling air from the holes spreads spanwise sufficiently to reach this midway line. In the high Tu case, this spreading occurred much more quickly, i.e., in comparatively fewer diameters downstream of the cooling holes, than in the low Tu case. This is consistent with increased turbulent mixing.

Schmidt and Bogard (1996) studied the effects of freestream turbulence and surface roughness on the effectiveness on a film-cooled flat plate, and reported streamwise and spanwise distributions. One key result from their experiments is that the range of optimum momentum flux ratios is much higher for a high freestream turbulence (Tu) flow than for a low Tu flow. Like Bons et al., they found that at high momentum flux ratio, high Tu improves the effectiveness, but at low momentum flux ratio high Tu decreases effectiveness.

Kohli and Bogard (1998) examined the temperature field around the injection area of a film-cooled flat plate using high and low freestream turbulence. They report the temperature contours up to 1.5 film cooling hole diameters away from the surface, in both the lateral and streamwise directions.

1.3. Density ratio

In an actual gas turbine engine the density ratio can be as high as 1.5–2.0. Forth et al. (1985), Pedersen et al. (1977), and Sinha et al. (1991) have all reported on the effect of density ratio on film cooling effectiveness on a flat plate in a low turbulence environment. Forth et al. (1985) concluded that blowing rate is not a good scaling parameter for effectiveness. Like Pedersen et al. (1977), they found that at high blowing rates (i.e., above the blowing rate for maximum effectiveness), the effectiveness scales well with velocity ratio. At low blowing rates (i.e., coolant flow still attached to the surface), they suggest momentum flux ratio as a scaling parameter. Sinha et al. (1991) suggest that the mass flux ratio is a good scaling parameter for low blowing rates (attached coolant flow), but did not report a good scaling parameter for high blowing rates.

The scaling apparently also depends on streamwise location. Pietrzyk et al. (1990) compare the velocity fields on a film-cooled flat plate for density ratios of unity and 2. Near the film cooling hole, they found that velocity ratio was the best scaling parameter for the velocity field; however, further downstream, blowing rate was the better scaling parameter for the velocity field. The correlations given by Baldauf et al. (1997) also show that the effect of density ratio depends on streamwise location.

Ekkad et al. (1997) have investigated the adiabatic effectiveness of a film-cooled flat plate with two density ratios with elevated freestream turbulence. The effects of density ratio on effectiveness they observed at elevated freestream turbulence were similar to those observed by Sinha et al. (1991) at low freestream turbulence. Although several research teams have addressed the problem, it remains unclear what the appropriate scaling parameters are for effectiveness at all blowing rates. However, the effect of freestream turbulence on effectiveness appears to be similar for different density ratios. Therefore, studies on the effect of freestream turbulence at a density ratio near unity are useful for applications where the density ratio is greater than unity.

1.4. Current research

The objective of the present work was not to simulate the density ratio seen in actual conditions, but rather to provide full-surface adiabatic effectiveness data over a film-cooled flat-plate geometry with and without significant freestream turbulence. A density ratio near unity was used. The wide-band thermochromic liquid crystal (TLC) technique was used to provide surface temperature measurement over a film-cooled surface. This technique not only provides good spatial resolution and relatively low uncertainty in temperature measurement, but also is an excellent flow visualization tool. The effects of freestream turbulence can be observed from photographs as well as measured directly from the color of the liquid crystal. It is hoped these data will be valuable for understanding flow interactions in film cooling and validation of CFD film-cooling codes.

2. Experimental facilities and instrumentation

2.1. Tunnel

The main flow of air, representing the gas flow over the turbine blade, comes from the test section of an open-circuit subsonic wind tunnel with a flow velocity of 25 m/s. A diagram is shown in Fig. 1. The wind tunnel has a test section 0.53 m long with a square cross-section of 0.305 m (12 in.) sides. The bottom and sides of the test section are constructed of 19.1 mm-thick Plexiglas. The flat plate test model forms the top surface of the test section. A trip strip of 6 mm-wide lead tape approximately 1 mm thick was placed across the width of the top of the wind tunnel at a location 0.15 m upstream of the test section in order to trip the boundary layer. For the low turbulence runs, the boundary layer velocity profile closely approximated the 1/7 power law profile. For the high freestream turbulence runs, the velocity varied approximately linearly from the surface to a point approximately 3 film-cooling hole diameters (38 mm) off the surface.

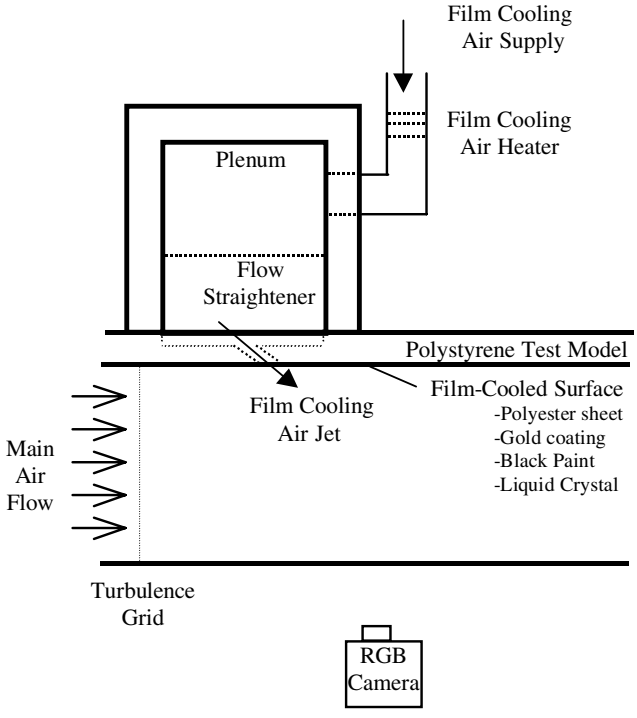

Fig. 1. Film cooling arrangement.

2.2. Grid

For the runs with high freestream turbulence, a grid constructed of square cross-section aluminum bars was installed in the wind tunnel 0.15 m upstream of the test section (see Fig. 1). The bars had a cross-section of 13 mm, and the edges were aerodynamically sharp. The turbulence intensity was 10% at the upstream edge of the film-cooling holes ($x/D = -2$), and exponentially decayed (Roach (1987)) to approximately 6% at the end of the test model at $x/D = 27$. Details of the grid construction and wind tunnel boundary layer profiles are given in Mayhew (1999).

2.3. Test model

The test model was constructed of 49 mm-thick polystyrene. Three cylindrical film-cooling holes were drilled at a 30° angle below the horizontal flat surface, as shown in Fig. 1. Thin plastic pipes of inside diameter 12.5 mm and thickness 1.6 mm were cemented into these holes to provide an aerodynamically smooth surface in the hole. The holes have a length to diameter ratio of 4.6. A diagram of the film-cooled surface, i.e., the bottom of the test model, is shown in Fig. 2. Both the main air flow and the cooling air flow are from left to right. Flat black paint (Hallcrest BBG-1) and microencapsulated TLCs (Hallcrest R24C10W/C17-10) were airbrushed on the film-cooled surface for surface temperature measurement and flow visualization.

The model is 0.305 m wide and 0.508 m long, large enough to form the entire top surface of the wind tunnel test section. The area from which TLC data were taken is smaller than the model. This was done to minimize side wall effects from the wind tunnel and the small bias in the liquid crystal due to variations in viewing and lighting angle.

A polyester sheet of thickness 0.2 mm with a microscopically thin layer of gold vacuum-deposited on the surface (''gold film'') was attached to the polystyrene test model. This polyester sheet provided an aerodynamically smooth flat plate surface. Since this model was also used for heat transfer measurements, the thin layer of gold served as an electric heater giving a nearly uniform heat flux. The electric heating was not used for the adiabatic effectiveness measurements. For adiabatic effectiveness, the cooling air is heated while the gold film electric heater power source is disconnected, and the model closely approximates an adiabatic surface. The amount of heating is kept small, so the density ratio does not differ greatly from 1.0—the density ratio used in the heat transfer runs (Mayhew et al., 2002).

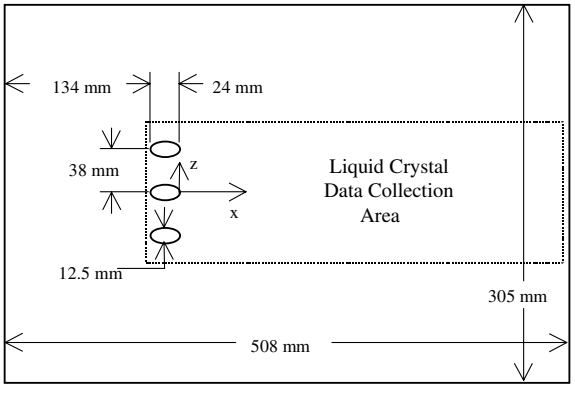

Fig. 2. Film-cooled surface.

2.4. Plenum

The plenum used to condition the film cooling air before it entered the cooling holes was a vertical right circular cylinder, of height 229 mm and diameter 105 mm, hollowed out of the same polystyrene material used to build the test model. Details are given in Mayhew (1999).

2.5. Thermistors

Four small-bead semi-conductor thermistors, Sensor Scientific Inc. Model S14B10325 with nominal resistance 10 kΩ at 25 °C, were used to measure all air temperatures. The thermistors were all calibrated together against the same standard, a digital platinum resistance thermometer with an absolute accuracy of ±0.1 °C. A Hewlett-Packard HP-3458A digital voltmeter was used to measure the resistance of the thermistors. The bias uncertainty of the resistance measurement was approximately ±2.5 Ω, or ±0.01 °C, which is negligible compared to other temperature uncertainties. The resolution of the temperature measurement was approximately 0.001 °C, again better than the temperature uncertainty.

2.6. Hot film

Air velocity and turbulence intensity measurements in the wind tunnel were made with a TSI IFA-300 anemometer using a TSI model 1218 hot film boundary-layer probe. A sampling rate of 10,000 Hz was used for a period of 1.6 s. A variable area rotameter, Omega Model FL-400A, was used to measure the flowrate of the cooling air.

2.7. Lights

A critical element of any experiment involving TLCs is the lighting. Four General Electric Cool White fluorescent bulbs of length 0.457 m (18 in.) were used to illuminate the test surface. Two standard desk lamps holding two bulbs each were attached to the bottom of the sides of the wind tunnel. Over each bulb an ultraviolet

(UV) filter, Spectracom model Spectrum 574, was placed in order to protect the liquid crystal from UV damage and to flatten out the spectrum from the cool white light, typically stronger in the blue wavelengths (Anderson, 1999).

3. Surface temperature measurement using thermochromic liquid crystals

3.1. Camera

A Sony/Donpisha XC-003 CCD camera with 480×640 pixel resolution is used to capture images of the film-cooled surface with the TLC colors. A Matrox Meteor RGB frame grabber in a Micron Millenia 166 MHz PC with 128 MB of RAM.

The frame grabber is a PC-based analog-to-digital converter for use specifically with cameras, and uses eight bits for each color. The result is a number from 0 to 255 for each color at each pixel; thus one image yields a $480\times640\times3$ array of approximately 0.9 MB. The following definition of hue, recommended by Hay and Hollingsworth (1996), has been used successfully by Baughn et al. (1999), and is used in this experiment,

$$\text{hue} = \frac{1}{2\pi}\arctan\left[\frac{(3)^{1/2}(G-B)}{(2R-G-B)}\right] \quad (1)$$

where R, G, and B represent the digital value of the red, green, and blue signals, respectively, from 0 to 255. The result is a number for hue between zero and unity.

3.2. Calibration

A calibration of the TLC used in this experiment was performed in situ using a 12.7 mm-thick aluminum plate as the top surface of the wind tunnel. This hue–temperature calibration curve is shown in Fig. 3. The calibration plate was airbrushed with the same black paint and TLC at the same time as the test models. Lighting conditions and viewing angle were identical for the calibration runs and data runs.

The aluminum plate was used for the calibration in order to provide a uniform temperature over a relatively large surface area. This has two particularly useful features. First, each photograph taken amounts to thousands of individual measurements of hue all at nearly the same known temperature. This improves the uncertainty of the hue measurement for that temperature (Mayhew, 1999). Second, the effect of different camera viewing angle is easily checked by comparing the hues at one end of the plate to the hues at the other end. The variation in hues over the area of interest was found to be negligibly small compared to the uncertainty in the hue measurement.

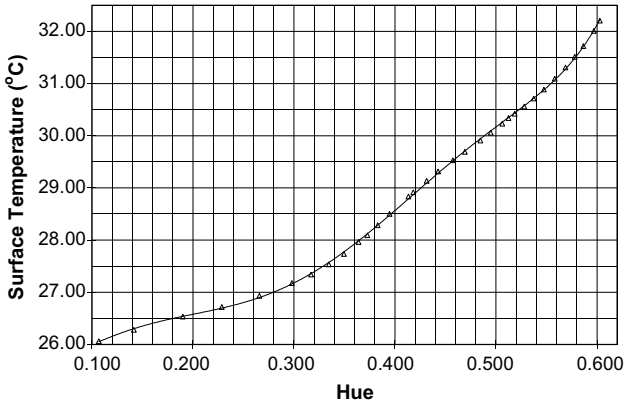

Fig. 3. Hue–temperature calibration curve for thermochromic liquid crystal.

As a further check on the hue–temperature relationship, after all experimental data had been taken, a bowl-shaped piece of polystyrene approximately 40 mm thick was held over the exit of the cooling holes in order to deflect the heated air jet back onto the model surface. The known temperature of the air jet was then compared to the hue on the model surface, with corrections for conduction losses in the polystyrene deflector.

Liquid crystal colors are strongly dependent on the angle at which the surface is viewed and the spectral distribution of the incident light. Since the TLC merely reflects the incident light, whatever irradiation is supplied to the surface affects what is reflected. Calibration is therefore done with identical lighting conditions and viewing angle.

3.3. Filtering

Using this calibration curve, the temperature can be computed at every pixel on the test model that has a measurable hue. However, there is typically a random uncertainty in the hue measurement as a result of noise in the camera/frame grabber system and non-uniformity in the TLC coating. In order to reduce this random uncertainty, a 5×5 median filter was applied to the RGB array. This median filter assigns to each pixel the value of the median of the 25 pixels in the 5×5 square of which it is the center. The resolution of the images after filtering is 3 mm by 3 mm (0.24 film cooling hole diameters) or better.

In summary, the hue of the color from the TLCs is computed from the individual R, G, and B components at every pixel, and is calibrated in situ against a known temperature using an aluminum calibration plate. Median filtering is used to reduce the random uncertainty of the measurement, at the expense of an acceptable loss in spatial resolution.

4. Operating conditions

$V_\infty = 25 \pm 0.5$ m/s,
$D = 12.5$ mm,
$T_{jet} = 50$ °C (typical), 34 °C (only used for $M = 0.5$ cases),
$V_{jet} = 12.5$, 25, 37.5 m/s,
$M = 0.46$, 0.92, 1.38,
$\delta_1/D = 0.12 \pm 0.04$ at $x/D = -2$ (leading edge of hole) for low Tu runs,
$\delta_1/\theta = 1.6 \pm 0.4$ at $x/D = -2$ (leading edge of hole) for low Tu runs,
$Re_D = 1.58E4$,
$Re_\theta = 1140 \pm 130$,
DR = 0.92 (for 50 °C jet), 0.97 (for 34 °C jet),
Tu = 0.1% (clean) or 10% (passive grid, 13.3 mm square cross-section), at cooling holes,
Length scale—macro: 18 ± 1 mm, micro: 5 ± 0.1 mm,
Upstream thermal boundary condition: nearly adiabatic (small conduction and radiation loss), steady-state.

5. Data reduction and uncertainty analysis

The adiabatic effectiveness η is defined by

$$\eta = \frac{T_{aw} - T_\infty}{T_{jet} - T_\infty} \tag{2}$$

Of the three variables on the right side of this equation, only T_∞ is measured directly, using the small-bead thermistor. The adiabatic wall temperature T_{aw} is found by measuring the temperature of the nearly adiabatic surface (using TLC) and correcting for the small radiation and 1D conduction terms. Lateral conduction effects were determined to be negligible. The jet temperature is found from the measured plenum temperature T_p (using a thermistor) with a small correction applied for conduction losses through the plenum wall. It should be noted that the temperature distribution of the air in the cooling hole is not known; the temperature quoted represents a bulk temperature of the jet. The typical plenum temperature was 50 °C, with a conduction correction varying from 0.05 to 0.2 °C, depending on the blowing rate.

The uncertainty of η and the relative contributions from each parameter for a typical data run are shown in Table 1. The surface temperature measurement dominates the uncertainty, followed by the freestream temperature measurement. Since the thermistors and liquid crystal were all calibrated against the same standard, their bias uncertainties are correlated, and therefore subtract out (Coleman and Steele, 1999).

Fig. 4 shows the variation of uncertainty with effectiveness and with jet temperature used. As for any effectiveness experiment, the uncertainty goes down as jet temperature increases. The results from the 50 °C jet runs are therefore preferred. Note that the actual uncertainty, not the percent, is tabulated above and shown in Fig. 4. The percent uncertainty decreases for higher values of η, from as high as 25% at $\eta = 0.05$ to as low as 5% at $\eta = 0.6$.

Table 1
Uncertainty in adiabatic effectiveness

Parameters	Typical Values	Px	Bx	η uncertainty
T_s	28.0 °C		0.27	0.019
T_∞	24.5 °C	0.2		0.011
h	75 W/m^2 K		20	0.005
hr	5.8 W/m^2 K		1	0.003
T_p	50.0 °C	0.2		0.003
η	0.25	0.012	0.020	0.023

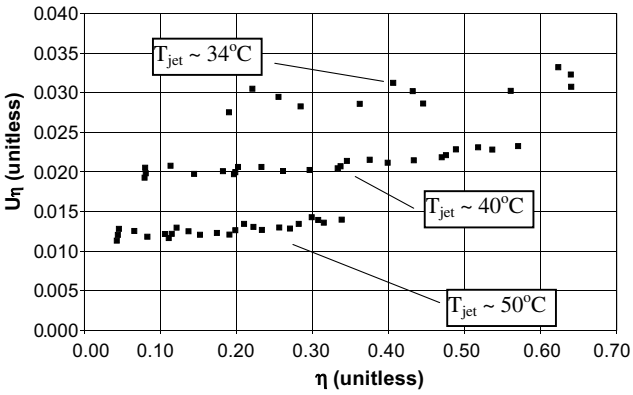

Fig. 4. Uncertainty in effectiveness.

Repeatability is generally within 0.02, with few exceptions. This is based on a comparison of the results at the three different jet temperatures (34, 40, and 50 °C). The effectiveness should not depend on the jet temperature for these small differences (density ratio varies from 0.92 to 0.97), so each jet temperature was an independent measurement of the same effectiveness.

6. Results

Note that due to the experimental technique used, the data are not accurate within 1 diameter of the film cooling holes. This is a conservative estimate to ensure the effects of conduction from the plastic cooling hole are negligible. Note also that for clarity of presentation the contour plots only include contours that are multiples of 0.05; images may contain data slightly higher than the highest contour shown, and slightly lower than the lowest shown. The temperature limits on the TLC (26.0–32.0 °C in this experiment), the jet temperature, and the freestream temperature determine the minimum and maximum values of effectiveness that can be measured in a given test. Since the freestream temperature

varied from 23.5 to 26.2 °C for different runs, the minimum and maximum values of effectiveness are not the same for each run.

Note too that the "coolant" used in these experiments is actually heated air. This is done for simplicity in the experimental design. The terms "heating air" and "cooling air" are used interchangeably in this paper.

In the raw RGB images shown in Fig. 5, the colors correspond to the surface temperature. The surface is very nearly adiabatic. Thus a red color indicates a low temperature and therefore a low effectiveness; blue indicates a higher temperature and therefore higher effectiveness.

Fig. 5(a) ($M = 0.5$, Tu = 0.1%) shows the long thin black areas between colored areas are essentially unprotected. The cooling (heating in this experiment) air has little to no effect on these areas. They would be hot spots on a film-cooled turbine blade. Fig. 5(b) and (c) show the effects of jet lift-off as the blowing rate is increased to $M = 1.0$ and 1.5, respectively, leaving very little area protected by the cooling air. Fig. 5(d) ($M = 0.5$, Tu = 10%) shows that high freestream turbulence spreads the cooling air around, covering more area; accordingly, less of the area is at the highest temperature (blue). The cooling air has a similar amount of energy as the low turbulence case, but it is spread out over a larger area. Fig. 5(e) and (f) show how high freestream turbulence improves adiabatic effectiveness at high blowing rates; the areas covered by cooling air in Fig. 5(e) and (f) are obviously larger than the corresponding low turbulence cases in Fig. 5(b) and (c). It should be noted that, although the trend is clear, a precise comparison can not be made from the raw images due to minor differences in ambient conditions from one image to the next. These differences are accounted for in the data reduction and contour plots.

6.1. Contour plots—low Tu

The contours with $M = 0.5$ shown in Fig. 6 indicate a region of effectiveness approximately two diameters wide at the lowest measured effectiveness of 0.1. At this low blowing ratio, it appears that the holes are having little influence on one another with regards to the effectiveness distribution. Fig. 7 shows contours of effectiveness at lower values of x/D, again for $M = 0.5$, obtained by using a lower jet temperature (34 °C). When using the 50 °C jet, the experimental setup gave a maximum measurable value of effectiveness of approximately 0.25–0.3. For $M = 0.5$, these occurred well downstream of the hole. For other blowing ratios, the 50 °C jet provided sufficient coverage. Fig. 7 shows an effectiveness as high as 0.6 between 1 and 2 diameters downstream of the hole. There is some overlap between Figs. 6 and 7; for example, at $x/D = 12$, Fig. 6 shows an effectiveness of 0.3–0.32 and Fig. 7 shows 0.27–0.29. This difference is due to uncertainty in the results, but is within the 95% confidence limit. The higher jet temperature has the lower uncertainty.

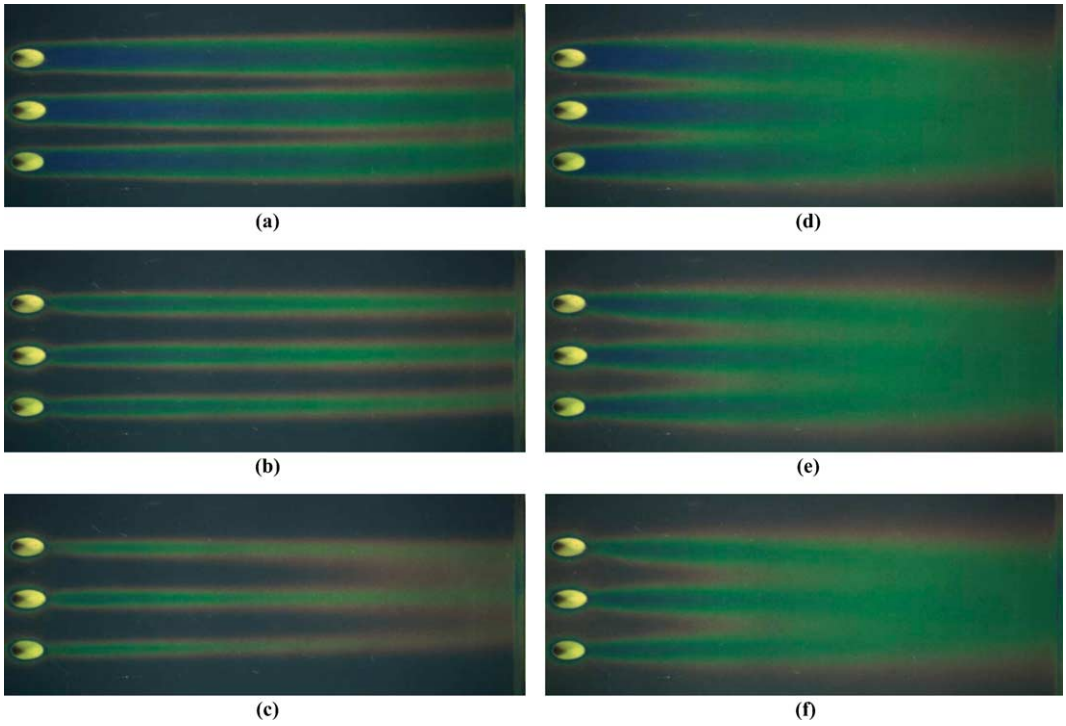

Fig. 5. Raw images of model at various blowing rates and low and high freestream turbulence levels: (a) $M = 0.5$, Tu = 0.1%, (b) $M = 1.0$, Tu = 0.1%, (c) $M = 1.5$, Tu = 0.1%, (d) $M = 0.5$, Tu = 10%, (e) $M = 1.0$, Tu = 10%, and (f) $M = 1.5$, Tu = 10%.

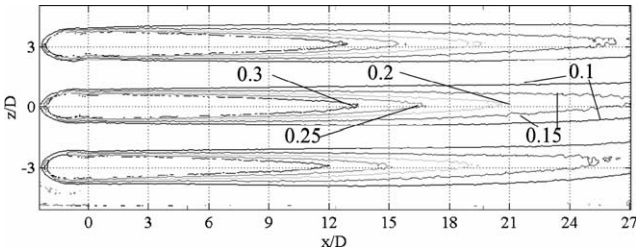

Fig. 6. Effectiveness contours, $M = 0.5$, Tu = 0.1%.

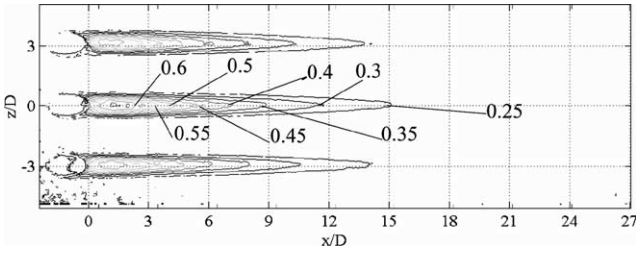

Fig. 7. Effectiveness contours, $M = 0.5$, Tu = 0.1%.

Fig. 8 shows similar contours for $M = 1.0$. At $x/D = 12$, the effectiveness is much lower, in the range of 0.15–0.16. Another noticeable item on these plots is that the 0.1 contour is only one diameter wide, compared to two diameters wide for $M = 0.5$. This is consistent with jet lift-off. The kidney vortices and associated entrained main flow (Mayhew et al., 2002) apparently sweep down at their outside edges, but then sweep up together in the middle of the jet. This would have the tendency to lift the jet away from the surface, and the higher blowing ratio exacerbates this by making the kidney vortices stronger. In addition, the higher momentum of the jet would tend to make it penetrate further into the mainstream, quite apart from kidney vortex effects, leaving less of the jet near the surface. The result is a narrower and shorter "footprint" of the jet on the film-cooled surface. The lift-off effect is greater at $M = 1.5$, shown in Fig. 9, with effectiveness of 0.1 or less at $x/D = 12$. Note also the good symmetry of the contours about the hole centerline.

In summary, for low freestream turbulence in the main flow, increased blowing ratio dramatically reduces

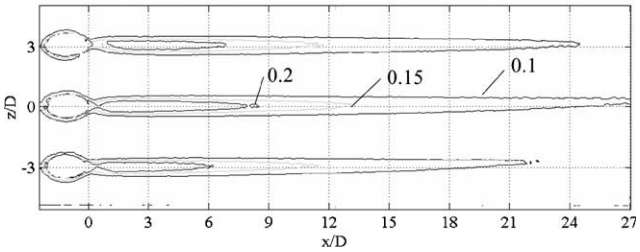

Fig. 8. Effectiveness contours, $M = 1.0$, Tu = 0.1%.

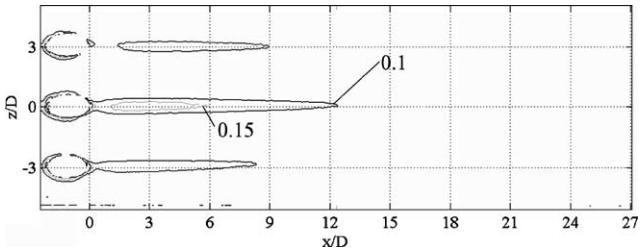

Fig. 9. Effectiveness contours, $M = 1.5$, Tu = 0.1%.

both the area of coverage of the film cooling air and the magnitude of the effectiveness. This is attributed to the jet lifting off the surface due to higher y-momentum in the jet and stronger kidney vortices.

6.2. High turbulence

Figs. 10 and 11 show the low blowing ratio, high turbulence effectiveness contour. Note in Fig. 10 that the $\eta = 0.1$ contour shown is approximately two diameters wide, like the low turbulence case, but that it stops at $x/D = 17$. The corresponding low turbulence contour (Fig. 6) continued past $x/D = 27$. The high freestream turbulence here has significantly shortened the distance that the cooling air travels downstream. This is attributed to the increased mixing of the coolant with the main flow due to the high turbulence. In the low turbulence case, the cooling air was laying down on the surface; the high freestream turbulence mixes it with the freestream air. This phenomenon is similar in appearance to the well-known jet lift-off at high blowing rates; a quick glance at Figs. 6 and 10 suggest that Fig. 10 is at

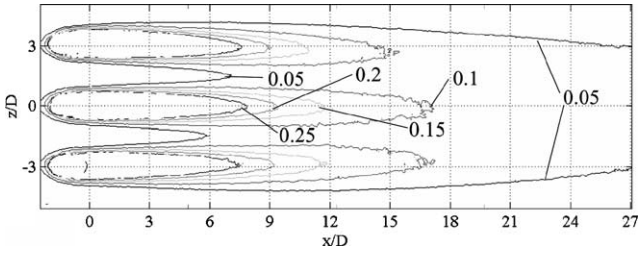

Fig. 10. Effectiveness contours, $M = 0.5$, Tu = 10%.

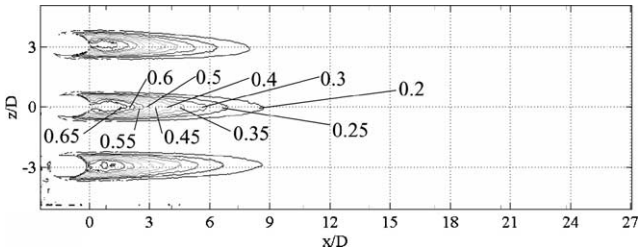

Fig. 11. Effectiveness contours, $M = 0.5$, Tu = 10% ($T_{jet} = 34$ °C.)

a higher blowing rate than Fig. 6, but they are both at $M = 0.5$, and jet lift-off does not occur at this blowing ratio. The shorter length of the effectiveness contours in Fig. 10 is due to the increased mixing as a result of the high freestream turbulence.

As in the low turbulence case, a lower jet temperature is needed to show the effectiveness contours at lower values of x/D. Fig. 11 shows these, indicating an effectiveness as high as 0.65 between 1 and 2 diameters downstream of the hole. Again, there is an overlap region; at $x/D = 9$, the 50 °C jet shows effectiveness of 0.21, and the 34 °C jet shows 0.19. Like the low turbulence case, this difference is attributed to uncertainty, and the 50 °C results have the lower uncertainty. In both cases the 34 °C jet gave a lower effectiveness.

Figs. 12 and 13 show the effectiveness contours for $M = 1.0$ and 1.5, respectively. The greater turbulent mixing tends to lay more cooling air down on the surface than the corresponding low turbulence case. In the low turbulence case, there was jet lift-off, so in this instance the increased mixing helps.

This increased mixing is further confirmed by examining the $\eta = 0.1$ contour in Figs. 12 and 13. At $M = 1.0$, Fig. 12 shows the $\eta = 0.1$ contour to be approximately one diameter wide, ending at $x/D = 18$. The corresponding low turbulence contour (Fig. 8) indicates the $\eta = 0.1$ contour is less than 1 diameter wide, and stops at $x/D = 21$. The high freestream turbulence has shortened but slightly widened the coverage area for $\eta = 0.1$. At $M = 1.5$, the high and low turbulence contours shown in Figs. 13 and 9 are almost identical with each other, but again the high turbulence case has an overall greater coverage area. "Evidently this occurs because the coolant jets are detached from the surface for these conditions and the greater dispersion of the coolant caused by the high freestream turbulence results in less detachment or movement of the coolant back to the surface" (Schmidt and Bogard (1996)). The current data are consistent with this hypothesis.

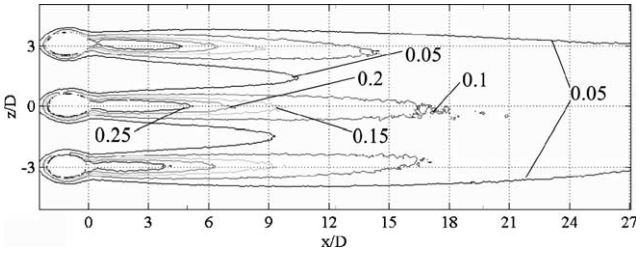

Fig. 12. Effectiveness contours, $M = 1.0$, Tu = 10%.

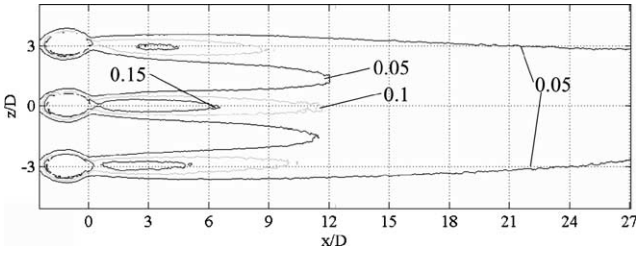

Fig. 13. Effectiveness contours, $M = 1.5$, Tu = 10%.

To quantify the effect of the high freestream turbulence, the $\eta = 0.1$ contours are compared for both the low and high turbulence cases. Table 2 lists the x/D location where the $\eta = 0.1$ contour crosses the centerline $z/D = 0$, and the maximum width of the $\eta = 0.1$ contour.

At low blowing ratio, the covered area is considerably longer in the low turbulence case, and the width is approximately the same. As blowing ratio is increased to $M = 1.5$, the low freestream turbulence loses its advantage. The high turbulence case has the same coverage at $\eta = 0.1$, but also has the full area coverage at $\eta = 0.05$.

An average effectiveness was computed over the rectangular area bounded by $-3 \leqslant z/D \leqslant 3$ and $3 \leqslant x/D \leqslant 15$. The results are shown in Table 3. It should be noted that the effectiveness in some portions of this rectangular area, particularly between the holes along $z/D = \pm 1.5$, was too low to be measured. Because of this lack of data, the averages shown in Table 3 have an uncertainty of approximately ±0.05.

In summary, at low blowing ratio, freestream turbulence clearly reduces the coverage area of the cooling air due to increased mixing with the main flow. However, at high blowing ratio, when much of the jet has lifted off in the low turbulence case, high freestream turbulence

Table 2
Comparison of $\eta = 0.1$ contour properties on three hole model at high and low freestream turbulence

Case	Maximum x/D	Maximum width of contour (hole diameters)
$M = 0.5$, low Tu	>27	2
$M = 0.5$, high Tu	15–17	2+
$M = 1.0$, low Tu	27	1
$M = 1.0$, high Tu	14–18	1+
$M = 1.5$, low Tu	12	0.75
$M = 1.5$, high Tu	12	0.75

Table 3
Area-averaged adiabatic effectiveness, three hole comparison with previously published data ($-3 \leq z/D \leq 3$ and $3 \leq x/D \leq 15$)

	I	M	η_{avg} low Tu	η_{avg} high Tu
Present (Tu 0.1%, 10%)	0.27	0.5	0.2	0.13
Present (Tu 0.1%, 10%)	1.1	1.0	0.1	0.1
Present (Tu 0.1%, 10%)	2.4	1.5	0.04	0.07
Schmidt et al. (1996) (Tu 0.2%)	0.25	0.63	0.25	N/A
Schmidt et al. (1996) (Tu 0.2%)	1	1.3	0.13	N/A

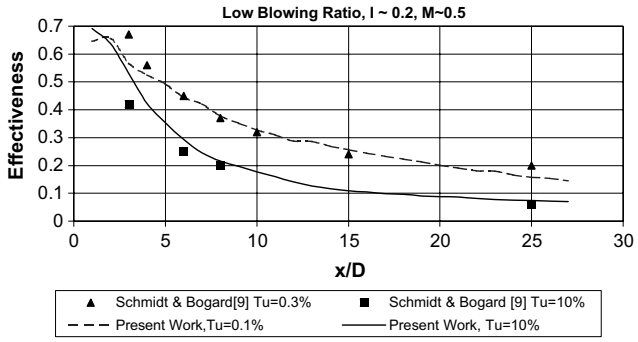

Fig. 14. Comparison of centerline effectiveness, low M.

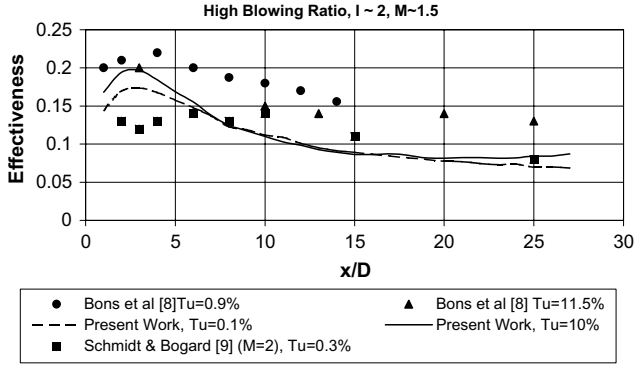

Fig. 15. Comparison of centerline effectiveness, high M.

turns its increased mixing into an asset, entraining some of the coolant that penetrates into the main flow and mixing it with the air near the surface. These results are consistent with those of Bons et al. (1994) and Schmidt and Bogard (1996), shown in Figs. 14 and 15.

7. Conclusions

This research has investigated the effects of freestream turbulence on adiabatic effectiveness on a film-cooled flat plate with three straight holes injected at an angle of 30°. The conclusions and recommendations are summarized below.

(1) In this research, a wide-band (~5 °C useful range) TLC was successfully used with the hue technique to measure surface temperatures at high resolution (0.2 film cooling hole diameters) and low uncertainty (±0.3 °C).
(2) The TLC method of measuring surface temperature has helped the visualization of cooling jet and main flow interactions on a film-cooled surface. This in turn is helpful for understanding and predicting film-cooling behavior. This paper contributes high-resolution color images that clearly show how the freestream turbulence spreads the cooling air around a larger area of the film-cooled surface.
(3) Median filtering was successfully used to reduce random uncertainty in temperature measurement at the expense of spatial resolution of the temperature measurement, which was acceptable in these experiments.
(4) In this research the calibration of hue versus temperature for wide-band TLC was performed in situ using the same lighting and camera positioned in the same locations as the experiment. This was found to be important to the successful use of wide-band TLCs, as it eliminates any variations in hue due to light source, illumination angle, and camera viewing angle, which can be substantial.
(5) High freestream turbulence has little effect on effectiveness for a blowing ratio of $M = 1.5$, but makes effectiveness worse for blowing ratios of $M = 0.5$ and 1.0.
(6) This research has provided full-surface contours of η for a film-cooled flat plate surface. It is hoped that this will be useful to the CFD community for code validation.

Acknowledgements

The support of the Aeronautics Research Center at the US Air Force Academy, and the AeroPropulsion and Power Directorate of the Air Force Laboratories, is gratefully acknowledged. The help of Professors Terry Jones (University of Oxford), Mike Owen (University of Bath) and Ken Van Treuren (Baylor University) is also acknowledged. This paper was first presented at the annual conference of the International Gas Turbine Institute, American Society of Mechanical Engineers, in Amsterdam, June 2002, paper number GT-2002-30172.

References

Anderson, M.Z., 1999. Thermochromic Liquid Crystal Thermography: Hysteresis, Illumination, and Imaging System Effects, Image Processing and Applications. Ph.D. Dissertation, University of California, Davis.

Baldauf, S., Schulz, A., Wittig, S., Scheurlen, M., 1997. An Overall Correlation of Film Cooling Effectiveness From One Row Of Holes. ASME paper 97-GT-79.

Baughn, J.W., Anderson, M.Z., Mayhew, J.E., Wolf, J.D., 1999. Hysteresis of thermochromic liquid crystal temperature measurement based on hue. ASME J. Heat Transfer 121, 1067–1072.

Bons, J.P., MacArthur, C.D., Rivir, R.B., 1994. The Effect of High Freestream Turbulence on Film Cooling Effectiveness. ASME Paper 94-GT-51.

Brittingham, R.A., Leylek, J.H., 1997. A Detailed Analysis of Film Cooling Physics Part IV: Compound-Angle Injection With Shaped Holes. ASME Paper 97-GT-272.

Coleman, H.W., Steele, W.G., 1999. Experimentation and Uncertainty Analysis for Engineers, second ed. John Wiley & Sons, New York, pp. 88–94.

Ekkad, S.V., Zapata, D., Han, J.C., 1997. Film effectiveness over a flat surface with air and CO_2 injection through compound angle holes using a transient liquid crystal image method. ASME J. Turbomach. 119, 587–593.

Forth, C.J.P., Loftus, P.J., Jones, T.V., 1985. The effect of density ratio on the film cooling of a flat plate. In: AGARD Conference Proceedings, CP 390, Paper 10.

Hay, J.L., Hollingsworth, D.K., 1996. A comparison of trichromic systems for use in the calibration of polymer-dispersed thermochromic liquid crystals. Experim. Therm. Fluid Sci. 12, 1–12.

Hyams, D.G., Leylek, J.H., 1997. A Detailed Analysis of Film Cooling Physics Part III: Streamwise Injection With Shaped Holes. ASME Paper 97-GT-271.

Kohli, A., Bogard, D.G., 1997. Adiabatic effectiveness, thermal fields, and velocity fields for film cooling with large angle injection. ASME J. Turbomach. 119, 352–358.

Kohli, A., Bogard, D.G., 1998. Effects of very high free-stream turbulence on the jet-mainstream interaction in a film cooling flow. ASME J. Turbomach. 120, 785–790.

Mayhew, J.E., 1999. An Experimental Investigation of the Effects of Freestream Turbulence on Film Cooling Using Thermochromic Liquid Crystal Thermography. Ph.D. Dissertation, University of California, Davis.

Mayhew, J.E., Baughn, J.W., Byerley, A.R., 2002. The Effect of Freestream Turbulence on Film Cooling Heat Transfer Coefficient. ASME Paper GT-2002-30173.

McGovern, K.T., Leylek, J.H., 1997. A Detailed Analysis of Film Cooling Physics Part II: Compound-Angle Injection With Cylindrical Holes. ASME Paper 97-GT-270.

Pedersen, D.R., Eckert, E.R.G., Goldstein, R.J., 1977. Film cooling with large density differences between the mainstream and the secondary fluid measured by the heat–mass transfer analogy. ASME J. Turbomach. 99, 620–627.

Pietrzyk, J.R., Bogard, D.G., Crawford, M.E., 1990. Effects of density ratio on the hydrodynamics of film cooling. ASME J. Turbomach. 112, 437–443.

Roach, P.E., 1987. The generation of nearly isotropic turbulence by means of grids. Heat Fluid Flow 8 (2), 82–92.

Schmidt, D.L., Bogard, D.G., 1996. Effects of Free-Stream Turbulence and Surface Roughness on Film Cooling. ASME Paper 96-GT-462.

Schmidt, D.L., Sen, B., Bogard, D.G., 1996. Film cooling with compound angle holes: adiabatic effectiveness. ASME J. Turbomach. 118, 807–813.

Sen, B., Schmidt, D.L., Bogard, D.G., 1996. Film cooling with compound angle holes: heat transfer. ASME J. Turbomach. 118, 800–806.

Sinha, A.K., Bogard, D.G., Crawford, M.E., 1991. Film cooling effectiveness downstream of a single row of holes with variable density ratio. ASME J. Turbomach. 113, 442–449.

Walters, D.K., Leylek, J.H., 1997. A Detailed Analysis of Film Cooling Physics Part I: Streamwise Injection With Cylindrical Holes. ASME Paper 97-GT-269.